A decoupling method for analysis of coupled RLC interconnects*

Jun Chen
ECE Department
University of Wisconsin, Madison

Lei He
ECE Department
University of Wisconsin, Madison

ABSTRACT

In this paper we present an efficient decoupling model for on-chip interconnect analysis. This model decouples multiple RLC transmission lines into independent lines with separate drivers and receivers. Based on this model we propose an efficient algorithm to solve the far end responses of multiple RLC lines. Experiments show good matching between our decoupling model and SPICE simulation. Based on the model, we further develop an N_{max} algorithm to quickly determine the noise amplitudes of far end responses. Experiments show that N_{max} algorithm gives conservative but reasonably accurate results compared to SPICE simulation.

Categories and Subject Descriptors

B.7.2 [**Integrated Circuits**]: Design Aids—*Verification*

General Terms

Design, Performance, Theory, Verification

1. INTRODUCTION

For integrated circuits in the deep submicron (DSM) technology, interconnects play an important role in determining the performance and signal integrity [1, 2]. An efficient on-chip interconnect analysis is critical to interconnect optimization at high-level design, logic synthesis and physical design, as circuit simulation is overkill and not affordable at these design stages. Closed-form formulae are particularly efficient and effective for these design stages. Previous works include formulae for delay [3, 4, 5, 6], noise [7, 8, 5], and time-domain response [9, 10]. The interconnect inductance is considered in [6, 9, 10], but not in [3, 5, 7, 8].

However, none of these papers consider the coupling inductance between interconnects. This may severely underestimate the interconnect noise and leads to large errors of the interconnect delay. Recently, two formulae were developed with consideration of the coupling inductance. One formula computes the coupling noise voltage in two identical RLC lines [11]. It is assumed that one wire (the aggressor) is switching, and the other stays quiet. Further, both lines are open-ended without drivers and receivers, and are loosely coupled, i.e., the noise can be ignored for the aggressor. These assumptions limit its application. The other formula computes the time-domain response for two identical lines with drivers and receivers [12]. It uses modal analysis [13, 14, 15, 16] to decouple two coupled lines into two independent lines, each with an independent driver and an independent receiver, and is able to consider arbitrary input signal combinations. However, it is not clear how to solve multiple lines by closed-form formulae.

In this paper, We first propose a decoupling model to decouple multiple transmission lines into a set of decoupled lines with separated drivers and receivers. Based on this model we develop an interconnect analysis algorithm to solve far end waveforms for multiple interconnects. Further, we developed an efficient N_{max} algorithm to quickly solve the noise amplitude of the far end response.

*The project is partially supported by NSF CAREER Award CCR-0093273, Intel and SUN Microsystems

GLSVLSI'02, April 18-19, 2002, New York, New York, USA.

2. WAVEFORM ANALYSIS

In this section we propose a decoupling model for multiple transmission lines and solve their far end responses.

2.1 Preliminaries

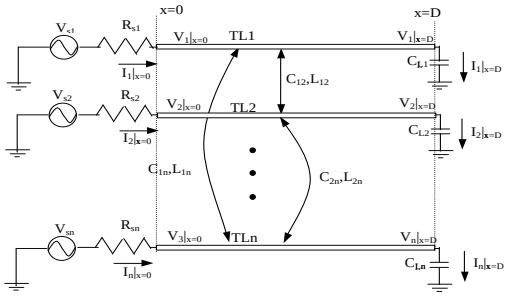

Figure 1: n coupled identical transmission lines with drivers and receivers.

In this paper we study multiple identical transmission lines which are aligned in a homogeneous dielectrics. We assume all transmission lines have a same cross section, there-

fore have a same unit length wire resistance. We also assume that all lines have identical drivers and receivers. However we do not require these lines have a uniform spacing or are routed in the same layer.

Figure 1 illustrate our circuit model. We assume n transmission lines, with drivers at $x = 0$ and receivers at $x = D$. A driver is modeled by a voltage source V_s with a source resistance R_s. A receiver is modeled by a load capacitance C_L. For the multiple wires in the figure 1, we denote input vector to the drivers as $\mathbf{V_s} = (V_{s1}, V_{s2}, \ldots, V_{sn})^T$, source resistance vector as $\mathbf{R_s} = (R_{s1}, R_{s2}, \ldots, R_{sn})^T$ and load capacitance vector as $\mathbf{C_L} = (C_{L1}, C_{L2}, \ldots, C_{Ln})^T$. Under our assumption, $R_{s1} = R_{s2} = \ldots = R_{sn}$ and $C_{L1} = C_{L2} = \ldots = C_{Ln}$. We consider the parasitics of the transmission lines such as unit length inductance $\mathbf{L}$, unit length capacitance $\mathbf{C}$, unit length resistance $\mathbf{R}$ and unit length conductance $\mathbf{G}$, all of which are $n \times n$ matrices. We also define the voltage vector of the transmission lines as $\mathbf{V}(x)(= (V_1(x), V_2(x), \ldots, V_n(x))^T)$ and the current vector as $\mathbf{I}(x)(= (I_1(x), I_2(x), \ldots, I_n(x))^T)$, with $0 \le x \le D$. For the simplicity of presentation, we will simply use $\mathbf{V}$ for $\mathbf{V}(x)$ and $\mathbf{I}$ for $\mathbf{I}(x)$.

$\mathbf{V}(x)$ is related to $\mathbf{I}(x)$ by

$$-\frac{d}{dx}\begin{pmatrix}\mathbf{V}\\ \mathbf{I}\end{pmatrix} = \begin{pmatrix}\mathbf{0} & \mathbf{Z}\\ \mathbf{Y} & \mathbf{0}\end{pmatrix}\begin{pmatrix}\mathbf{V}\\ \mathbf{I}\end{pmatrix} \quad (1)$$

where $\mathbf{Z}(= \mathbf{R} + s\mathbf{L})$ and $\mathbf{Y}(= \mathbf{G} + s\mathbf{C})$. We assume $\mathbf{G} = \mathbf{0}$, thus $\mathbf{Y} = s\mathbf{C}$. By circuit analysis, the boundary condition for this system can be described as,

$$\mathbf{V}|_{x=0} = \mathbf{V}_s - \mathbf{R}_s\mathbf{I}|_{x=0} \quad (2)$$

$$\mathbf{I}|_{x=D} = s\mathbf{C}_L\mathbf{V}|_{x=D}. \quad (3)$$

$\mathbf{Y} \cdot \mathbf{Z}$ normally are not diagonalized, so elements of $\mathbf{V}$ and $\mathbf{I}$ couple with each other. We denote this coupled system as $\mathcal{S}$.

System $\mathcal{S}$ can be transformed to a new system $\hat{\mathcal{S}}$ by linear transformation. For an invertible matrix $\mathbf{M}$, we define the following transformation for transmission lines and source voltages,

$$\begin{pmatrix}\hat{\mathbf{V}}(x)\\ \hat{\mathbf{I}}(x)\end{pmatrix} = \begin{pmatrix}\mathbf{M^{-1}} & \mathbf{0}\\ \mathbf{0} & \mathbf{M^{-1}}\end{pmatrix}\begin{pmatrix}\mathbf{V}(x)\\ \mathbf{I}(x)\end{pmatrix} \quad (4)$$

$$\hat{\mathbf{V}}_s = \mathbf{M^{-1}}\mathbf{V}_s. \quad (5)$$

We call $\mathbf{M}$ the transformation matrix. We denote all the quantities in $\hat{\mathcal{S}}$ with symbol '$\hat{}$'.

We have proved the following lemmas:

Lemma 1: For system $\hat{\mathcal{S}}$,

$$\hat{\mathbf{R}} = \mathbf{R} \quad (6)$$

$$\hat{\mathbf{C}} = \mathbf{M^{-1}}\mathbf{C}\mathbf{M} \quad (7)$$

$$\hat{\mathbf{L}} = \mathbf{M^{-1}}\mathbf{L}\mathbf{M} \quad (8)$$

$$\hat{\mathbf{Z}} = \hat{\mathbf{R}} + s\hat{\mathbf{L}} \quad (9)$$

$$\hat{\mathbf{Y}} = s\hat{\mathbf{C}}. \quad (10)$$

$$\hat{\mathbf{R}}_s = \mathbf{R}_s \quad (11)$$

$$\hat{\mathbf{C}}_L = \mathbf{C}_L \quad (12)$$

where $\hat{\mathbf{R}}, \hat{\mathbf{C}}, \hat{\mathbf{L}}, \hat{\mathbf{Z}}$ and $\hat{\mathbf{Y}}$ are the unit length resistance, capacitance, inductance, impedance and conductance of transmission lines in $\hat{\mathcal{S}}$, and $\hat{\mathbf{V}}_s, \hat{\mathbf{R}}_s$ and $\hat{\mathbf{C}}_L$ are the source voltages, source resistances and load capacitances in $\hat{\mathcal{S}}$.

Lemma 2: $\mathbf{V}$ and $\mathbf{I}$ can be expressed in $\hat{\mathbf{V}}$ and $\hat{\mathbf{I}}$ as

$$\begin{pmatrix}\mathbf{V(x)}\\ \mathbf{I(x)}\end{pmatrix} = \begin{pmatrix}\mathbf{M} & \mathbf{0}\\ \mathbf{0} & \mathbf{M}\end{pmatrix}\begin{pmatrix}\hat{\mathbf{V}}(x)\\ \hat{\mathbf{I}}(x)\end{pmatrix} \quad (13)$$

Lemmas 1 and 2 can be easily proved by applying the linear transformation and assumptions that the unit length resistance, source resistances and load capacitances are identical for all transmission lines. We will include the proof in an online full version of our paper[21].

2.2 Decoupling Transformation

In [12] two identical coupled lines with identical drivers and receivers have been successfully decoupled into two independent lines, each with an independent driver and an independent receiver. The transformation is carried out by the following matrix

$$\mathbf{M} = \begin{pmatrix}\frac{\sqrt{2}}{2} & \frac{\sqrt{2}}{2}\\ \frac{\sqrt{2}}{2} & -\frac{\sqrt{2}}{2}\end{pmatrix} \quad (14)$$

In this paper we develop a decoupling method for multiple lines. We define $\mathbf{M_C}$ as the eigenvector matrix of capacitance matrix $\mathbf{C}$ (each column in an eigenvector matrix is an eigenvector of the original matrix). Similarly we define $\mathbf{M_L}$ as the eigenvector matrix of inductance matrix $\mathbf{L}$. We have the following theorem,

Theorem 1: By the transformation defined in section 2.1, $\mathbf{M_C}$ or $\mathbf{M_L}$ transforms (1) into n independent transmission lines, each with an independent driver and an independent receiver.

Sketch of Proof: Because of the symmetry of $\mathbf{C}$ and $\mathbf{L}$, we just prove the case $\mathbf{M} = \mathbf{M_C}$. To prove Theorem 1, we only need to prove that all the matrices on the *lhs* of (6)-(12) are diagonalized. First, all transmission lines, drivers and receivers are identical, so according to (6),(11) and (12), $\hat{\mathbf{R}}$, $\hat{\mathbf{R}}_s$ and $\hat{\mathbf{C}}_L$ are obviously diagonalized. Second, because $\mathbf{M}$ is the eigenvector matrix of $\mathbf{C}$, $\hat{\mathbf{C}}$ and further $\hat{\mathbf{Y}}$ are diagonalized according to (7) and (10). Finally it has been shown[17, 16] for transmission lines in homogeneous dielectric

$$\mathbf{LC} = \frac{1}{c^2}, \quad (15)$$

where c is the speed of light in the dielectric. Because we assume homogeneous dielectric in this paper, (15) holds in system $\mathcal{S}$ (defined in section 2.1). From (15) we have

$$\mathbf{LC} = \mathbf{M^{-1}}\mathbf{L}\mathbf{M} \cdot \mathbf{M^{-1}}\mathbf{C}\mathbf{M} = \hat{\mathbf{L}}\hat{\mathbf{C}} = \frac{1}{c^2}. \quad (16)$$

Because $\hat{\mathbf{C}}$ is diagonalized, $\hat{\mathbf{L}}$ and therefore $\hat{\mathbf{Z}}$ must also be diagonalized. Because all the matrices on *lhs* of (6)-(12) are diagonalized, there is no coupling between transformed lines in system $\hat{\mathcal{S}}$. Also each of them has its independent driver and receiver. The detailed proof will be given in [21].

Further, we have following theorem:

Theorem 2: There are closed-form solutions to $\mathbf{M}_C$ and $\mathbf{M}_L$ for up to four transmission lines, and numerical solutions for arbitrary number of transmission lines.

To prove this, one just need note that there is closed-form solution for eigenvectors of matrix less than fifth order. We will include the detailed proof in [21]. Well-developed and efficient numerical algorithms for calculating eigenvectors of a matrix can be found in [18, 16].

2.3 Far End Response

Based on the theorems in section 2.2, we developed an interconnect analysis algorithm to compute the far end responses of the coupled interconnects. We summarize this algorithm in table 1.

According to our decoupling model each decoupled line i has n input components V_s^{ij} according to (5) . Each V_s^{ij} is due to the original input to the original line j. Because of linearity of the system, the waveform at the far end of an decoupled line i will be the linear combination of the responses of all the input components V_s^{ij} of line i. We define the output component A_{ij} as the response of V_s^{ij} at the far end of the decoupled line i. There are n such output components for each decoupled line due to n coupled lines. The total far end response of decoupled line i is the sum of A_{ij}. After obtaining the waveforms of the decoupled lines, as shown in (13), we can obtain the waveform of any original coupled line as the linear combinations of the waveforms of all n decoupled lines. With a closed-form solution to A_{ij}, we are able to further develop a quick noise computation algorithm in section 3.

Algorithm Interconnect analysis
1. Calculate $\mathbf{M_C}$ or $\mathbf{M_L}$.
2. Calculate $\hat{\mathbf{R}}$, $\hat{\mathbf{L}}$, $\hat{\mathbf{C}}$, $\hat{\mathbf{R}}_s$ and $\hat{\mathbf{C}}_L$ according to (6)-(15).
3. Convert the $\mathbf{V}_s$ to $\hat{\mathbf{V}}_s$ according to (5).
4. Calculate $\hat{V}_j$ and $\hat{I}_j$ for each independent line j separately, $j = 1, 2, \ldots, n$.
5. Calculate $\mathbf{V}$ and $\mathbf{I}$ by (13).
end

Table 1: Algorithm for interconnect analysis.

2.4 Experiment Results

To verify our decoupling model, we have applied the algorithm in table 1 to a number of interconnect structures. In order to verify our derivation of the decoupling model, in step 4 of the algorithm, we use SPICE simulation to solve the response for each decoupled line. We then compare the results given by our decoupling algorithm to the results from SPICE simulation over the coupled transmission line model. The wires used in the experiments all are $1.6\mu m$ wide, $1.09\mu m$ thick and $3000\mu m$ long. The ground plane is $25\mu m$ wide and has the same length as wires. Distance between the top of the ground plane and the bottom of the wires is 4.15μ. The parasitics are extracted by the Hspice 2D field solver. Note that the matrices $\mathbf{M_C}$ and $\mathbf{M_L}$ are solved analytically for structures consisting of less than five nets, but is solved numerically for structures consisting of more nets. The results from our experiments show an good matching between SPICE simulation and our model. For the simplicity of presentation of input signal patterns, we use '+', '-', and '0' to represent rising signals, falling signals and quiet victim respectively. For example, (+0-) means line 1 switches from 0 to 1, line 2 is quiet, and line3 switches from 1 to 0. In figure 2 we show the geometry for six lines in two layers and the waveform of line 2 and line 6. From figure 2, we can see that the waveforms from our decoupled model are almost indistinguishable from those obtained by direct SPICE simulation. More examples are given in [21].

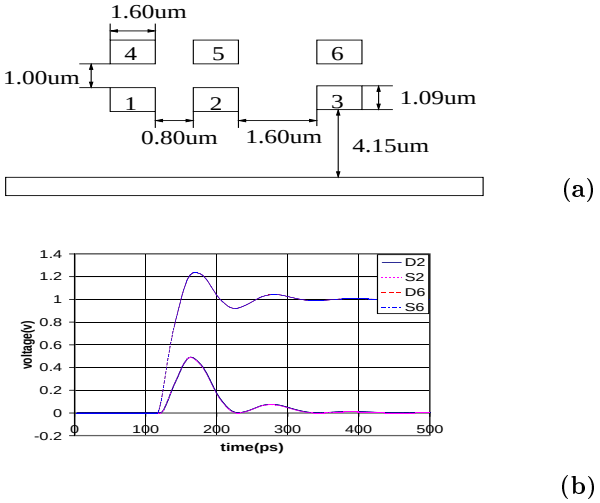

Figure 2: Six wires in two layers with input of (+0+0++). (a) Geometry; (b) Comparison of waveforms of wire 2 and wire 6 between decoupling model($D2$ and $D6$) and SPICE simulation($S2$ and $S6$).

3. NOISE ANALYSIS

Based on the interconnect analysis algorithm in section 2.3, we develop an efficient noise analysis algorithm (N_{max} algorithm) to compute the noise amplitudes at the far end of a coupled RLC interconnect structure in this section.

3.1 Terminologies

Let $V(t)|_{x=D}$ be the waveform at a receiver, and $V_f = \lim_{t\to\infty} V(t)$. For quiet lines and lines switching from 0 to 1, we define the overshoot as $V(t)|_{x=D} - V_f$ when $V(t)|_{x=D} \geq V_f$ and $t \geq T_0$, and define undershoot as $V_f - V(t)|_{x=D}$ when $V(t)|_{x=D} \leq V_f$ and $t \geq T_0$, where T_0 is the time instant of the first overshoot peak. Similarly, for lines switching from 1 to 0, we define overshoot as $V_f - V(t)|_{x=D}$ when $V(t)|_{x=D} \leq V_f$ and $t \geq T_0$, and define undershoot as $V(t)|_{x=D} - V_f$ when $V(t)|_{x=D} \geq V_f$ and $t \geq T_0$. We further define N^+_{max} as the maximum overshoot and N^-_{max} as the maximum undershoot. Figure 3 shows the overshoots and undershoots on an aggressor and a victim. We will develop closed-form

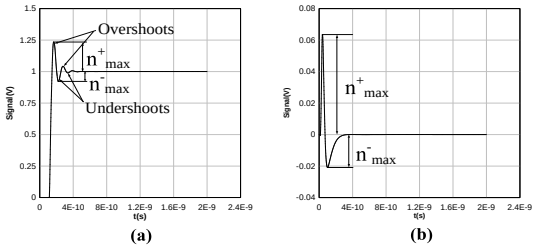

Figure 3: Overshoot and undershoot. (a):An aggressor line switching from 0 to 1. (b):A victim line.

solution to N^+_{Max} and N^-_{Min} at the receivers of three lines with arbitrary arriving times and input patterns. We call our solution N_{max} model. Note that N_{max} model can be applied to more than three transmission lines, even though the closed-form solution may not exist for all cases.

3.2 N_{max} Algorithm

In N_{max} model, we first divide the time domain into small regions such that all the mathematical terms in derivatives of all the output components A_{ij} (defined in section 2.3) in the decoupling model are monotonic in each and every region. We call these regions *monotonic regions*. Then we search the noise peaks in the monotonic regions. Finally, N^+_{max} and N^-_{max} are picked from these noise peaks over all monotonic regions. In Table 2 we summarize the method.

Algorithm N_{max}
begin
1. Define monotonic regions;
For each monotonic region,
2. search the noise peak;
3. Update N^+_{max} and N^-_{max} according to definitions.
end

Table 2: N_{max} algorithm

Below we show how to define monotonic regions. First, we use the three-pole closed-form formula from [12] to solve a single output component. We modified the original formula into the following equation so that it can consider none-zero initial conditions:

$$V_c(t)|_{x=D} = \sum_{1\le m\le 3}(v_f - v_i)k_m[\frac{{t_r}^{-1}}{p_m(p_m+{t_r}^{-1})}e^{p_m t} - \frac{1}{p_m}+\frac{1}{p_m+{t_r}^{-1}}e^{-{t_r}^{-1}t}] + v_i \quad (17)$$

where p_m are the poles, k_m are corresponding coefficients, v_i and v_f are the initial and final values of the corresponding input component, and t_r is the rising time. p_1 and k_1 are real. p_2 and p_3 are complex conjugate, i.e., $p_2 = p_a + p_b I$ and $p_3 = p_a - p_b I$. Similarly, $k_2 = k_a + k_b I$ and $k_3 = k_a - k_b I$. Signal arriving time is assumed to be $t = 0$.

Then, we obtain the derivative of (17)

$$\frac{dV_c(t)}{dt}|_{x=D} = (v_f - v_i)(k_1\frac{t_r^{-1}}{p_1+t_r^{-1}}e^{p_1 t} + 2|k_2|\frac{t_r^{-1}}{|p_2+t_r^{-1}|}cos(p_b t+\beta)e^{p_a t} + \sum_{1\le m\le 3}k_m\left[-\frac{t_r^{-1}}{p_m+t_r^{-1}}e^{-t_r^{-1}t}\right]) \quad (18)$$

where β is the phase of term $\frac{k_2}{p_2+t_r^{-1}}$. We only need to consider the cosine terms in (18), because exponential terms are always monotonic. By setting $\frac{d}{dt}[cos(p_b t+\beta)e^{p_a t}] = 0$, we obtain the time as

$$t_e^m = \frac{(m+\frac{1}{2})\pi - \gamma}{p_a} + t_d \quad (19)$$

where m is an integer and t_d is the corresponding signal arrival time. γ is the phase of term $\frac{k_2 p_2}{p_2+t_r^{-1}}$. We solve t_e^m's for all output components, then we sort all t_e^m's in an increasing order as $t_i (i = 1, 2, \ldots)$. The monotonic regions are defined as $\mathcal{T}_i = (t_i, t_{i+1})$, $i = 1, 2, \ldots$.

Finally, the peaks' positions are given by the roots of the equation $\frac{dV(t)}{dt} = 0$. Here V(t) is the far end response of a transmission line. We approximate $\frac{dV(t)}{dt}$ in the monotonic region $(t(i), t(i+1))$ with a straight line passing through points $(t_i, \frac{dV(t)}{dt}|_{t=t_i})$ and $(t_{i+1}, \frac{dV(t)}{dt}|t = t_{i+1}))$. Under this approximation, the noise peaks only exist in the region, where $\frac{dV(t)}{dt}|_{t=t_i} \cdot \frac{dV(t)}{dt}|_{t=t_{i+1}} \le 0$. The time correspondent to the peak is

$$t_p = t_1 + \frac{t(i)-t(i+1)}{\frac{dv}{dt}|_{t=t(i)} - \frac{dv}{dt}|_{t=t(i+1)}} \cdot \frac{dv}{dt}|_{t=t(i)} \quad (20)$$

Because the noise decreases exponentially, we do not need to search all peaks of V to find N^+_{max} and N^-_{max}. The number of peaks needed to be searched can be decided by the arrival times and the number of lines. Let t_0 be the time of the first overshoot peak, and t_f be the fly time. We search up to four peaks (two maxima and two minima) or up to $t_0 + 4t_f$, whichever is smaller. In case there is no overshoot peak, a maximum time limit such as a half clock cycle is set.

3.3 Experiment Results

In this subsection, we compare the N_{max} with the most accurate model - SPICE simulation over SPICE physical model (in short, SPICE RLC model).

First we compare our model to SPICE simulation to show the efficiency of our model. In table 3 we show some experiment results of running time for both SPICE simulation and our model. In this comparison, bus structures of different sizes are constructed. The wires are $2000\mu m$ long, $0.8\mu m$ wide, $1.0\mu m$ thick. Spacings between wires are $0.8\mu m$ uniformly. For the SPICE model, each wire is modeled with $100\mu m$ long π segments. For each configuration we do 10 runs and get the average. The experiment is running on a SUN machine. From the results, we can see that the speedup of N_{max} over SPICE RLC model is roughly 10 for large number of interconnects. However the speedup is over 100 for three coupled interconnects. A decomposition method has been presented in [20] to estimate the noise of a wide bus structures based on the solution to a number of three-net structures, where our N_{max} model is highly efficient.

Table 3: Running time comparison

bus size	N_{max}	SPICE
3	0.014s	1.6s
16	1.6s	13.6s
32	17.4s	186.4s

Next we compare the noise value from N_{max} with SPICE RLC model. To illustrate the importance of inductance effect, we further compare the SPICE RLC model with SPICE simulation over distributed RC model (in short, SPICE RC model). For the SPICE RC model, we construct a π-circuit for every $50\mu m$-long wire segment. In our experiment, we use three transmission lines with wire width of $1.6\mu m$ and wire height of $0.8\mu m$. We present all the experiment parameters in Table 4, and enumerate all combinations of these parameters in experiments.

Table 4: Experiment configurations

Spacing(μm)	0.8, 1.6
Length(μm)	1000,2000,3000
Input pattern	all combinations
Arrival time(ps)	(0,0,20), (0,0,0), (40,0,0),(30,0,15)
Technology (μm)	0.07 ($R_s = 100\Omega$,$C_L = 40fF$,$T_r = 20ps$) 0.10 ($R_s = 150\Omega$,$C_L = 60fF$,$T_r = 33ps$)

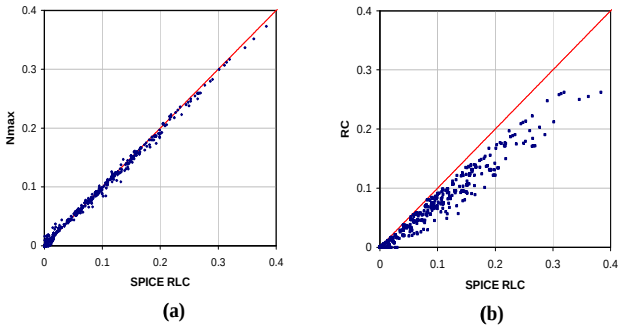

Figure 4: Comparison of overshoot of victim lines at x=D with SPICE RLC model. (a) N_{max} model; (b) SPICE RC model. The straight line is accurate solution.

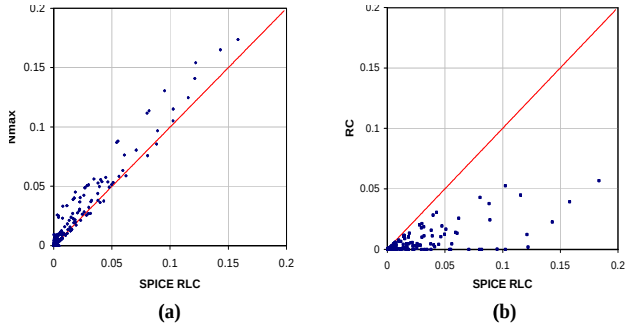

Figure 5: Comparison of overshoot of aggressor lines at x=D with SPICE RLC model. (a) N_{max} model; (b) SPICE RC model. The straight line is accurate solution

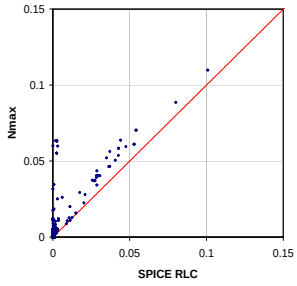

Figure 6: Comparison of undershoot of aggressor lines at x=D from N_{max} model with SPICE RLC model. The straight line is accurate solution.

We compare the N_{max} model and SPICE RLC model for N^{+}_{max} of victim lines in Figure 4(a), and compare the SPICE RC model and SPICE RLC in Figure 4(b). One can easily see that the N_{max} model obtains results very close to accurate solutions (SPICE RLC model), but the RC model severely underestimates the noise. The underestimation is especially severe for large noise values, and may cause design failure in practice.

We compare the N_{max} model and SPICE RLC model for N^{+}_{max} of aggressor lines in Figure 5(a). The N_{max} model leads to a relatively larger error for aggressors than the error for victims, but it is conservative for most cases and is useful to guide design optimization for signal integrity. Even though the N^{+}_{max} noise of aggressors can be up to 15% of Vdd, it was ignored in previous work such as [19, 11]. Further, we compare the SPICE RC model and SPICE RLC model for N^{+}_{max} of aggressor lines in Figure 5(b). Again the RC model severely underestimates the noise amplitude, and is not safe to guide design optimization.

Finally, we compare the N_{max} model with SPICE RLC model for N^{-}_{max} in aggressors in Figure 6. The N_{max} model is reasonably accurate except for very small noise that can be ignored in practice. Again, the N_{max} model is conservative for almost all cases and is useful to guide design optimization for signal integrity.

4. DISCUSSION AND CONCLUSION

In this paper, we have developed a decoupling model to decouple multiple RLC transmission lines into independent lines, each with an independent driver and an independent receiver. Therefore, each decoupled line can be analyzed separately. Based on this decoupling model, we have developed a closed-form N_{max} model to compute a variety of noise amplitudes in three coupled transmission lines. Note that the N_{max} model is applicable to an arbitrary number of transmission lines, even though the closed-form solution may not exist for all cases. Extensive experiments have shown that our N_{max} model computes noise values for victim lines with a high accuracy, and provides conservative noise for aggressor lines. Note that the noise value for aggressor lines can be up to 15% of Vdd, even though it was often ignored by previous work.

We plan to extend the N_{max} model to consider unaligned lines with non-identical drivers and receivers, and apply the N_{max} model to interconnect design and verification.

5. REFERENCES

[1] J. Cong, L. He, C.-K. Koh, and P. H. Madden, "Performance optimization of VLSI interconnect layout," *Integration, the VLSI Journal*, vol. 21, pp. 1–94, 1996.

[2] K. L. Shepard and V. Narayanan, "Noise in deep submicron digital design," in *Proc. Int. Conf. on Computer Aided Design*, 1996.

[3] W. C. Elmore, "The transient response of damped linear networks with particular regard to wide-band amplifiers," *Journal of Applied Physics*, vol. 19, pp. 55–63, Jan. 1948.

[4] A. B. Kahng, K. Masuko, and S. Muddu, "Analytical delay model for VLSI interconnects under ramp input," in *Proc. Int. Conf. on Computer Aided Design*, pp. 30–36, Nov. 1996.

[5] T. Sakuri, "Closed-form expressions for interconnection delay, coupling, and crosstalk in vlsi's," *IEEE Trans. Electron Devices*, pp. 118–124, Jan. 1993.

[6] Y. I. Ismail, E. G. Friedman, and J. L. Neves, "Equivalent elmore delay for RLC trees," *IEEE Trans. on Computer-Aided Design of Integrated Circuits and Systems*, 2000.

[7] A. Vittal, L. H. Chen, K. W. M. Marek-Sadowska, and S. Yang, "Crosstalk in VLSI interconnections," *IEEE Trans. on CAD-12*, pp. 1817–1824, Dec. 1999.

[8] D. Z. Z. J. Cong and P. V. Srinivas, "Improved crosstalk modeling for noise constrained interconnect optimization," in *Proc. Asia South Pacific Design Automation Conf.*, 2001.

[9] Y. Gao and D. F. Wong, "Optimal shape function for a bi-directional wire under elmore delay model," in *Proc. Int. Conf. on Computer Aided Design*, pp. 622–627, 1997.

[10] B. Krauter, R. Gupta, J. Willis, and L. T. Pileggi, "Transmission line synthesis," in *Proc. Design Automation Conf*, pp. 358–363, 1995.

[11] K. T. Tang and E. G. Friedman, "Interconnect coupling noises in CMOS VLSI circuits," in *Proc. Int. Symp. on Physical Design*, pp. 48–53, 1999.

[12] L. Yin and L. He, "An efficient analytical model of coupled on-chip rlc interconnects," in *Proc. Asia South Pacific Design Automation Conf.*, 2001.

[13] F. Chang, "Transient analysis of lossless coupled transmission lines in a nonehomogeneous dielectric medium," *IEEE Trans. MTT*, pp. 616–627, Sept. 1970.

[14] V. K. Tripathi and J. B. Rettig, "A spice model for multiple coupled microstrips and other transmission lines," *IEEE Trans. on Microwave Theory and Techniques*, Dec 1985.

[15] A. R. Djordjevic, T. K. Sarkar, and R. F. Harrinton, "Time domain response of multiconductor transmission lines," *Proc. IEEE*, June 1987.

[16] K. D. Granzow, *Digital Transmission Lines*. Oxford University Press, 1998.

[17] L. Dworsky, *Modern transmission Line theory and Applications*. John Wiley & Sons Press, 1979.

[18] E. Anderson etc., *LAPACK User's Guide*, 1999.

[19] A. B. Kahng and S. Muddu, "Optimal equivalent circuits for interconnect delay calculations using moments," in *Proc. European Design Automation Conf.*, pp. 164–169, Sept. 1994.

[20] K. M. Lepak, I. Luwandi, and L. He, "Simultaneous shield insertion and net ordering for coupled RLC nets under explicit noise constraint," *in Proc. Design Automation Conf.*, 2001.

[21] J. Chen, and L. He, "A decoupling method for analysis of multiple coupled RLC interconnects", http://eda.ece.wisc.edu/publications.html.